

# Resumming Cosmic Perturbations

**Sabino Matarrese**

Dipartimento di Fisica “G. Galilei”, Università di Padova and INFN, Sezione di Padova, via Marzolo 8, I-35131, Padova, Italy

E-mail: [sabino.matarrese@pd.infn.it](mailto:sabino.matarrese@pd.infn.it)

**Massimo Pietroni**

INFN, Sezione di Padova, via Marzolo 8, I-35131, Padova, Italy

E-mail: [massimo.pietroni@pd.infn.it](mailto:massimo.pietroni@pd.infn.it)

**Abstract.** Renormalization Group (RG) techniques have been successfully employed in quantum field theory and statistical physics. Here we apply RG methods to study the non-linear stages of structure formation in the Universe. Exact equations for the power-spectrum, the bispectrum, and all higher order correlation functions can be derived for any underlying cosmological model. A remarkable feature of the RG flow is the emergence of an intrinsic UV cutoff, due to dark matter velocity dispersion, which improves the convergence of the equations at small scales. As a consequence, the method is able to follow the non-linear evolution of the power-spectrum down to zero redshift and to length-scales where perturbation theory fails. Our predictions accurately fit the results of  $N$ -body simulations in reproducing the “Baryon Acoustic Oscillations” features of the power-spectrum, which will be accurately measured in future galaxy surveys and will provide a probe to distinguish among different dark energy models.

## 1. Introduction

Precision Cosmology relies on the capability of accurately extracting cosmological parameters from measurements of observables related to Cosmic Microwave Background (CMB) temperature anisotropy and polarization as well as to the Large-Scale Structure (LSS) of the Universe. In the CMB context, the tool allowing a comparison of data and theory, at the percent level, is perturbation theory (PT). One would however like to reach the same level of precision also in the study of the other main cosmological probe, the LSS of the Universe. In particular, the location and amplitude of Baryon Acoustic Oscillations (BAO), wiggles in the matter power-spectrum produced by the coupling of baryons to radiation by Thomson scattering in the early universe, for wavenumbers in the range  $k \simeq 0.05 - 0.3 \text{ hMpc}^{-1}$ , have the potential to constrain the expansion history of the Universe and the nature of the Dark Energy [1]. BAO's have recently been detected both in the 2dF and SDSS surveys data [2], and are going to be measured in the near future in a series of high-redshift surveys [3].

Due to the higher degree of non-linearity of the underlying density fluctuations compared to those relevant for the CMB, accurate computations of the power-spectrum in the BAO region is challenging, and has so far been best afforded by means of high-resolution  $N$ -body simulations (see, e.g. Ref. [4]). In particular, the study of BAO to constrain Dark Energy models requires a precision of a few percent in the theoretical predictions for the matter power-spectrum in the relevant wavenumber range [5]. Including higher orders in PT [6] is known to give a poor performance in this range, while all available fitting functions for the non-linear power-spectrum (e.g. refs. [7, 8]) are incapable to reach the required level of accuracy [4], leaving  $N$ -body simulations as the only viable approach to the problem.

Recently, however, PT has experienced a renewed interest, mainly motivated by two reasons. First, next generation galaxy surveys [3] are going to measure the power-spectrum at large redshift, where the fluctuations are still in the linear regime and 1-loop PT is expected to work [5]. Second, Crocce and Scoccimarro [9, 10] have shown that the perturbative expansion can be reorganized in a very convenient way, which allows the use of standard tools of field theory, like Feynman diagrams. They managed to compute the two-point correlator between density or velocity field fluctuations at different times (the 'propagator') by resumming an infinite class of diagrams at all orders in PT. Other approaches can be found in Ref. [11].

In this paper, we will present a new approach to the problem, based on Renormalization Group (RG) techniques developed in quantum field theory and statistical physics [12]. We will give the full details of the formulation of the method and of its application to the computation of the power-spectrum in the BAO region, whose results have been recently presented in Ref. [13].

RG methods are particularly suited to physical situations in which there is a separation between the scale where one is supposed to control the 'fundamental' theory and the scale where measurements are actually made. Starting from the fundamental

scale, the RG flow describes the gradual inclusion of fluctuations at scales closer and closer to the one relevant to measurements. The new fluctuations which are included at an intermediate step, feel an effective theory, which has been ‘dressed’ by the fluctuations already included. In the present case, the RG flow will start from small wavenumbers  $k$ , where linear theory works, to reach higher and higher  $k$ .

One of the most important results of our analysis is that an intrinsic ultra-violet (UV) cutoff emerges from the RG flow, which suggest that the non-linear gravitational evolution itself implies a small-scale smoothing, so that our description can work also on fairly non-linear scales. The main result of this paper is the evaluation of the non-linear matter power-spectrum in a standard  $\Lambda$ CDM model, including a very accurate fit of the BAO features obtained in  $N$ -body simulations, down to zero redshift and to length-scales where any previous analytical or semi-analytical techniques have failed. Moreover, our approach allows a straightforward extension to more general cosmologies with dynamical dark energy.

The plan of the paper is as follows. In Section 2 we introduce the equations that govern the dynamics of self-gravitating dark matter in the fluid limit and, following Ref. [9], we recast them in the compact form of a single non-linear equation, for a suitable field doublet in Fourier space. In Section 3 we obtain the generating functional of  $n$ -point correlation functions for our system in the form of a path-integral which incorporates the statistics of initial conditions (here assumed to be Gaussian, for simplicity). The general formulation of the RG equations is given in Section 4. In Sects. 5 and 6 we derive the equations and present our solutions for the non-linear propagator and PS, respectively. Conclusions and future prospects are discussed in Sect. 7.

## 2. Eulerian theory revisited

The distribution of a gas of DM particles of mass  $m$  is described by the function  $f(\mathbf{x}, \mathbf{p}, \tau)$ , where  $\mathbf{x}$  represents the comoving spatial coordinate,  $\mathbf{p}$  is given by

$$\mathbf{p} = am \frac{d\mathbf{x}}{d\tau},$$

( $a$  being the scale factor) and  $\tau$  is the conformal time.

The evolution of  $f$  is governed by the collisionless Boltzmann equation, a.k.a. the Vlasov equation,

$$\frac{\partial f}{\partial \tau} + \frac{\mathbf{p}}{am} \cdot \nabla f - am \nabla \phi \cdot \nabla_{\mathbf{p}} f = 0. \quad (1)$$

$\phi$  is the gravitational potential which, on subhorizon scales, obeys the Poisson equation,

$$\nabla^2 \phi = \frac{3}{2} \mathcal{H}^2 \delta, \quad (2)$$

with  $\mathcal{H} = d \log a / d\tau$  and  $\delta$  the mass-density fluctuation,

$$\int d^3 \mathbf{p} f(\mathbf{x}, \mathbf{p}, \tau) \equiv \rho(\mathbf{x}, \tau) \equiv \bar{\rho}(\tau) [1 + \delta(\mathbf{x}, \tau)], \quad (3)$$

having assumed an Einstein-de Sitter background cosmology.

A full solution of the –non-linear and non-local– Vlasov equation is a formidable task. A more affordable strategy is to take *moments* of the distribution functions. Along with the zeroth order one, defined in Eq. (3), one can define the infinite tower of higher order moments,

$$\begin{aligned} \int d^3\mathbf{p} \frac{p_i}{am} f(\mathbf{x}, \mathbf{p}, \tau) &\equiv \rho(\mathbf{x}, \tau) v_i(\mathbf{x}, \tau) \\ \int d^3\mathbf{p} \frac{p_i p_j}{a^2 m^2} f(\mathbf{x}, \mathbf{p}, \tau) &\equiv \rho(\mathbf{x}, \tau) v_i(\mathbf{x}, \tau) v_j(\mathbf{x}, \tau) + \sigma_{ij}(\mathbf{x}, \tau) \\ &\dots \end{aligned} \quad (4)$$

The definitions above, once inserted in the Vlasov equation, give rise to an infinite hierarchy of equations involving moments of higher and higher order [6]. The system can be truncated by setting to zero the stress tensor  $\sigma_{ij}$ . Although the latter term would arise as soon as orbit-crossing appears in the non-linear evolution of our collisionless system, this procedure, dubbed ‘single stream approximation’, is formally self-consistent, since no non-vanishing  $\sigma_{ij}$  is generated by the above set of moment equations once it is set to zero in the initial conditions. Moreover, as we will see in the following, an intrinsic UV cutoff emerges from the RG flow.

In this case, one is left with just two equations

$$\begin{aligned} \frac{\partial \delta}{\partial \tau} + \nabla \cdot [(1 + \delta)\mathbf{v}] &= 0, \\ \frac{\partial \mathbf{v}}{\partial \tau} + \mathcal{H}\mathbf{v} + (\mathbf{v} \cdot \nabla)\mathbf{v} &= -\nabla\phi, \end{aligned} \quad (5)$$

which are the continuity and Euler equations, respectively.

Defining, as usual, the velocity divergence  $\theta(\mathbf{x}, \tau) = \nabla \cdot \mathbf{v}(\mathbf{x}, \tau)$ , and going to Fourier space, Eqs. (5) read

$$\begin{aligned} \frac{\partial \delta(\mathbf{k}, \tau)}{\partial \tau} + \theta(\mathbf{k}, \tau) &+ \int d^3\mathbf{q} d^3\mathbf{p} \delta_D(\mathbf{k} - \mathbf{q} - \mathbf{p}) \alpha(\mathbf{q}, \mathbf{p}) \theta(\mathbf{q}, \tau) \delta(\mathbf{p}, \tau) = 0, \\ \frac{\partial \theta(\mathbf{k}, \tau)}{\partial \tau} + \mathcal{H}\theta(\mathbf{k}, \tau) + \frac{3}{2}\mathcal{H}^2\delta(\mathbf{k}, \tau) &+ \int d^3\mathbf{q} d^3\mathbf{p} \delta_D(\mathbf{k} - \mathbf{q} - \mathbf{p}) \beta(\mathbf{q}, \mathbf{p}) \theta(\mathbf{q}, \tau) \theta(\mathbf{p}, \tau) = 0. \end{aligned} \quad (6)$$

The non-linearity and non-locality of the Vlasov equation survive in the two functions

$$\alpha(\mathbf{p}, \mathbf{q}) = \frac{(\mathbf{p} + \mathbf{q}) \cdot \mathbf{p}}{p^2}, \quad \beta(\mathbf{p}, \mathbf{q}) = \frac{(\mathbf{p} + \mathbf{q})^2 \mathbf{p} \cdot \mathbf{q}}{2p^2q^2}, \quad (7)$$

which couple different modes of density and velocity fluctuations.

Setting  $\alpha(\mathbf{p}, \mathbf{q}) = \beta(\mathbf{p}, \mathbf{q}) = 0$ , the equations can be solved as

$$\begin{aligned} \delta(\mathbf{k}, \tau) &= \delta(\mathbf{k}, \tau_i) \left( \frac{a(\tau)}{a(\tau_i)} \right)^m, \\ -\frac{\theta(\mathbf{k}, \tau)}{\mathcal{H}} &= m \delta(\mathbf{k}, \tau), \quad (m = 1, -3/2), \end{aligned} \quad (8)$$

where we recognize the growing ( $m = 1$ ) and decaying ( $m = -3/2$ ) modes of the linear order equations of standard cosmological PT in the Newtonian limit.

Following Crocce and Scoccimarro [9, 10] one can write Eqs. (6) in a compact form. First, we introduce the doublet  $\varphi_a$  ( $a = 1, 2$ ), given by

$$\begin{pmatrix} \varphi_1(\mathbf{k}, \eta) \\ \varphi_2(\mathbf{k}, \eta) \end{pmatrix} \equiv e^{-\eta} \begin{pmatrix} \delta(\mathbf{k}, \eta) \\ -\theta(\mathbf{k}, \eta)/\mathcal{H} \end{pmatrix}, \quad (9)$$

where the time variable has been replaced by the logarithm of the scale factor,

$$\eta = \log \frac{a}{a_{in}},$$

$a_{in}$  being the scale factor at a conveniently remote epoch, were all the relevant scales are well inside the linear regime. Notice that, compared with the definition used by Crocce and Scoccimarro, we have a  $e^{-\eta}$  factor overall, such that the linear growing mode corresponds to  $\varphi_a = \text{const}$ .

Then, we define a *vertex* function,  $\gamma_{abc}(\mathbf{k}, \mathbf{p}, \mathbf{q})$  ( $a, b, c, = 1, 2$ ) whose only non-vanishing elements are

$$\begin{aligned} \gamma_{121}(\mathbf{k}, \mathbf{p}, \mathbf{q}) &= \frac{1}{2} \delta_D(\mathbf{k} + \mathbf{p} + \mathbf{q}) \alpha(\mathbf{p}, \mathbf{q}), \\ \gamma_{222}(\mathbf{k}, \mathbf{p}, \mathbf{q}) &= \delta_D(\mathbf{k} + \mathbf{p} + \mathbf{q}) \beta(\mathbf{p}, \mathbf{q}), \end{aligned} \quad (10)$$

and  $\gamma_{121}(\mathbf{k}, \mathbf{p}, \mathbf{q}) = \gamma_{112}(\mathbf{k}, \mathbf{q}, \mathbf{p})$ .

The two equations (6) can now be rewritten as

$$(\delta_{ab} \partial_\eta + \Omega_{ab}) \varphi_b(\mathbf{k}, \eta) = e^\eta \gamma_{abc}(\mathbf{k}, -\mathbf{p}, -\mathbf{q}) \varphi_b(\mathbf{p}, \eta) \varphi_c(\mathbf{q}, \eta), \quad (11)$$

where

$$\Omega = \begin{pmatrix} 1 & -1 \\ -3/2 & 3/2 \end{pmatrix},$$

and repeated indices/momenta are summed/integrated over. Besides the vertex, the other building block of the perturbation theory we are going to use is the linear retarded *propagator*, defined as the operator giving the evolution of the field  $\varphi_a$  from  $\eta_b$  to  $\eta_a$ ,

$$\varphi_a^0(\mathbf{k}, \eta_a) = g_{ab}(\eta_a, \eta_b) \varphi_b^0(\mathbf{k}, \eta_b), \quad (\eta_a > \eta_b) \quad (12)$$

where the subscript “0” indicates solutions of the linear equations (obtained in the  $e^\eta \gamma_{abc} \rightarrow 0$  limit).

The propagator  $g_{ab}(\eta_a, \eta_b)$  can be explicitly computed by solving the equation

$$(\delta_{ab} \partial_{\eta_a} + \Omega_{ab}) g_{bc}(\eta_a, \eta_b) = \delta_{ac} \delta_D(\eta_a - \eta_b), \quad (13)$$

with causal boundary conditions (see [9]), getting,

$$g_{ab}(\eta_a, \eta_b) = \left[ \mathbf{B} + \mathbf{A} e^{-5/2(\eta_a - \eta_b)} \right]_{ab} \theta(\eta_a - \eta_b), \quad (14)$$

with  $\theta$  the step-function, and

$$\mathbf{B} = \frac{1}{5} \begin{pmatrix} 3 & 2 \\ 3 & 2 \end{pmatrix} \quad \text{and} \quad \mathbf{A} = \frac{1}{5} \begin{pmatrix} 2 & -2 \\ -3 & 3 \end{pmatrix}. \quad (15)$$

The growing ( $\varphi_a \propto \text{const.}$ ) and the decaying ( $\varphi_a \propto \exp(-5/2\eta_a)$ ) modes can be selected by considering initial fields  $\varphi_a$  proportional to

$$u_a = \begin{pmatrix} 1 \\ 1 \end{pmatrix} \quad \text{and} \quad v_a = \begin{pmatrix} 1 \\ -3/2 \end{pmatrix}, \quad (16)$$

respectively.

To extend the validity of this approach to  $\Lambda$ CDM, we will reinterpret the variable  $\eta$  as the logarithm of the linear growth factor of the growing mode, i.e.  $\eta = \ln(D^+/D_{in}^+)$ . This approximation has been shown to accurately fit N-body simulations for different cosmologies (e.g. Refs. [5, 14]). A closer look at the problem shows that this approximation relies on the ansatz of setting artificially to one the quantity  $e(\Omega_m) \equiv \Omega_m/f^2$ , with  $f = d \ln D_+/d \ln a$ , which is anyway very close to unity for most of the history of the Universe in a wide class of cosmologies. Moreover, as shown in Ref. [10], the slight deviation of  $e(\Omega_m)$  from unity would only affect the decaying mode, thus making the above approximation extremely accurate.

### 3. Generating functionals

The aim of this section is to apply methods familiar in quantum field theory to construct generating functionals for quantities like the power-spectrum, bispectrum, propagator and any other object of interest. The starting point is to write down an action giving the equation of motion (11) at its extrema. One can realize that a new, auxiliary, doublet field  $\chi_a$  has to be introduced to this aim, and that the action is given by

$$S = \int d\eta [\chi_a(-\mathbf{k}, \eta) (\delta_{ab} \partial_\eta + \Omega_{ab}) \varphi_b(\mathbf{k}, \eta) - e^\eta \gamma_{abc}(-\mathbf{k}, -\mathbf{p}, -\mathbf{q}) \chi_a(\mathbf{k}, \eta) \varphi_b(\mathbf{p}, \eta) \varphi_c(\mathbf{q}, \eta)] . \quad (17)$$

The introduction of the auxiliary field  $\chi_a$  is required by the bilinear term being first order in the ‘time’ derivative  $\partial_\eta$ . Indeed, a term of the form  $\varphi_a \partial_\eta \varphi_a$  would vanish upon integration by parts. Using Eq. (13), the bilinear part in the first line of the action can be also written as

$$S_2 = \int d\eta_a d\eta_b \chi_a(-\mathbf{k}, \eta_a) g_{ab}^{-1}(\eta_a, \eta_b) \varphi_b(\mathbf{k}, \eta_b) . \quad (18)$$

Varying the action (17) with respect to  $\chi_a$  gives precisely Eq. (11), while varying with respect to  $\varphi_a$  gives an equation solved by  $\chi_a = 0$ . The rôle of the  $\chi_a$  field is not merely that of allowing to write the action above, but more physically, it is related to the statistics of initial conditions, as we will see below. In the following, in order to simplify the notation, we will omit momentum dependence when it is obvious.

Being the system classical, the probability of having a field  $\varphi_a(\eta_f)$  at time  $\eta_f$ , starting with an initial condition  $\varphi_a(0)$  is a (functional) delta function:

$$P[\varphi_a(\eta_f); \varphi_a(0)] = \delta [\varphi_a(\eta_f) - \bar{\varphi}_a[\eta_f; \varphi_a(0)]] , \quad (19)$$

where  $\bar{\varphi}_a[\eta_f; \varphi_a(0)]$  is the solution to the equation of motion (11) with initial condition  $\varphi_a(0)$ . Using the action (17), where the  $\chi_a$  field enters linearly, the delta function can be given a path integral representation,

$$P[\varphi_a(\eta_f); \varphi_a(0)] = \mathcal{N} \int \mathcal{D}''\varphi_a \mathcal{D}\chi_b e^{iS}, \quad (20)$$

where the double prime on the measure for  $\varphi_a$  means that it is kept fixed at the two extrema  $\eta = 0$  and  $\eta = \eta_f$ . In the following, the field-independent normalization  $\mathcal{N}$  will be set to unity.

We then define a generating functional by following the standard procedure, *i.e.* by introducing sources for  $\varphi_a$  and  $\chi_b$  and by summing over all the possible final states, *i.e.*,

$$Z[J_a, K_b; \varphi_a(0)] \equiv \int \mathcal{D}\varphi_a(\eta_f) \int \mathcal{D}''\varphi_a \mathcal{D}\chi_b \times \exp \left\{ i \int_0^{\eta_f} d\eta \chi_a (\delta_{ab} \partial_\eta + \Omega_{ab}) \varphi_b - e^\eta \gamma_{abc} \chi_a \varphi_b \varphi_c + J_a \varphi_a + K_a \chi_a \right\}. \quad (21)$$

Finally, since we are interested in statistical systems, we average the probabilities over the initial conditions with a statistical weight function for the physical fields  $\varphi_a(0)$ ,

$$Z[J_a, K_b; C's] = \int \mathcal{D}\varphi_a(0) W[\varphi_a(0), C's] Z[J_a, K_b; \varphi_a(0)]. \quad (22)$$

In general, the initial weight can be expressed in terms of the initial  $n$ -point correlations as [15]

$$W[\varphi_a(0), C's] = \exp \left\{ -\varphi_a(\mathbf{k}, 0) C_a(\mathbf{k}) - \varphi_a(\mathbf{k}_1, 0) C_{ab}(\mathbf{k}_1, \mathbf{k}_2) \varphi_b(\mathbf{k}_2, 0) + \varphi_a(\mathbf{k}_1, 0) \varphi_b(\mathbf{k}_2, 0) \varphi_c(\mathbf{k}_3, 0) C_{abc}(\mathbf{k}_1, \mathbf{k}_2, \mathbf{k}_3) + \dots \right\}. \quad (23)$$

In the case of Gaussian initial conditions, the only non-zero initial correlation is the quadratic one, and the weight function reduces to the form

$$W[\varphi_a(0), C_{ab}] = \exp \left\{ -\frac{1}{2} \varphi_a(\mathbf{k}, 0) C_{ab}(k) \varphi_b(-\mathbf{k}, 0) \right\}, \quad (24)$$

where

$$\mathbf{C}^{-1}_{ab}(k) = P_{ab}^0(k) \equiv w_a w_b P^0(k), \quad (25)$$

with  $P^0(k)$  the initial power-spectrum and the two-component vector  $w_a$  is a combination of  $u_a$  and  $v_a$  in Eq. (16) describing the initial mixture of growing and decaying modes [9]. In the following, we will restrict the initial conditions to the Gaussian case, Eq. (24), leaving the study of the effect of primordial non-Gaussianity to future work.

The linear theory limit,  $e^\eta \gamma_{abc} \rightarrow 0$ , corresponds to the tree-level of PT. In this limit the path integral can be explicitly computed. Performing first the  $\chi_a$  integral, and then the  $\int \mathcal{D}\varphi_a(\eta_f) \mathcal{D}''\varphi_a$  ones, we obtain [16]

$$Z_0[J_a, K_b; P^0] = \int \mathcal{D}\varphi_a(0) \exp \left\{ -\frac{1}{2} \varphi_a(\mathbf{k}, 0) (\mathbf{P}^{0^{-1}})_{ab}(k) \varphi_b(-\mathbf{k}, 0) + i \int_0^{\eta_f} d\eta J_a \tilde{\varphi}_a \right\}, \quad (26)$$

where  $\tilde{\varphi}_a$  is the solution of the classical equation of motion with source  $K_a$ ,

$$(\delta_{ab}\partial_\eta + \Omega_{ab})\tilde{\varphi}_b(\eta) = -K_a(\eta), \quad (27)$$

which is given by

$$\tilde{\varphi}_a(\eta_a) = \varphi_a^0(\eta_a) - \int d\eta_b g_{ab}(\eta_a, \eta_b) K_b(\eta_b), \quad (28)$$

with  $\varphi_a^0(\eta)$  the known sourceless zeroth-order solution, see Eq. (12).

The remaining integral on the initial conditions  $\varphi_a(0)$  can also be performed, leading to the result

$$Z_0[J_a, K_b; P^0] = \exp \left\{ - \int d\eta_a d\eta_b \left[ \frac{1}{2} J_a(\mathbf{k}, \eta_a) P_{ab}^L(k; \eta_a, \eta_b) J_b(-\mathbf{k}, \eta_b) + i J_a(\mathbf{k}, \eta_a) g_{ab}(\eta_a, \eta_b) K_b(-\mathbf{k}, \eta_b) \right] \right\}, \quad (29)$$

where  $P_{ab}^L$  is the power-spectrum evolved at linear order,

$$P_{ab}^L(k; \eta_a, \eta_b) = g_{ac}(\eta_a, 0) g_{bd}(\eta_b, 0) P_{cd}^0(k). \quad (30)$$

Starting from this explicit expression we can recover the results of linear theory. For instance, the power-spectrum,

$$\langle \varphi_a(\mathbf{k}, \eta_a) \varphi_b(\mathbf{k}', \eta_b) \rangle \equiv \delta(\mathbf{k} + \mathbf{k}') P_{ab}(k; \eta_a, \eta_b), \quad (31)$$

is given (at linear order) by the double derivative of  $Z_0$  with respect to the source  $J_a$ ,

$$\frac{(-i)^2}{Z_0} \frac{\delta^2 Z_0[J_a, K_b; P^0]}{\delta J_a(\mathbf{k}, \eta_a) \delta J_b(\mathbf{k}', \eta_b)} \Big|_{J_a, K_b=0} = \delta(\mathbf{k} + \mathbf{k}') P_{ab}^L(k; \eta_a, \eta_b). \quad (32)$$

Using Eq. (12) in (31) we recover the linear behavior of the power-spectrum, Eq. (30).

The cross-derivative gives the retarded propagator

$$\delta(\mathbf{k} + \mathbf{k}') g_{ab}(\eta_a, \eta_b) = \frac{i}{Z_0} \frac{\delta^2 Z_0[J_a, K_b; P^0]}{\delta J_a(\mathbf{k}, \eta_a) \delta K_b(\mathbf{k}', \eta_b)} \Big|_{J_a, K_b=0}. \quad (33)$$

Thus, from a single object,  $Z_0$ , we are able to obtain all the quantities of interest, that is, the propagator, the power-spectrum, and all higher order correlation functions, by taking appropriate derivatives of it with respect to the sources. The generalizations of Eqs. (32) and (33) to the power-spectrum and propagator of the full non-linear theory will be given in Eq. (43) below.

Turning the interaction  $\gamma_{abc}$  on, the generating functional (22) can be rewritten as

$$Z[J_a, K_b; P^0] = \exp \left\{ -i \int d\eta e^\eta \gamma_{abc} \left( \frac{-i\delta}{\delta K_a} \frac{-i\delta}{\delta J_b} \frac{-i\delta}{\delta J_c} \right) \right\} Z_0[J_a, K_b; P^0], \quad (34)$$

with  $Z_0$  given by Eq. (29). Higher orders in PT are obtained by expanding the exponential in powers of  $\gamma_{abc}$ . From this expression for  $Z$  one can read out the Feynman rules. The three fundamental building blocks, *i.e.* the propagator  $g_{ab}$ , the linearly evolved power-spectrum  $P_{ab}^L$ , and the trilinear vertex  $e^\eta \gamma_{abc}$ , can be represented by the Feynman diagrams in Fig. 1. Continuous and dashed lines indicate  $\varphi_a$  and  $\chi_a$



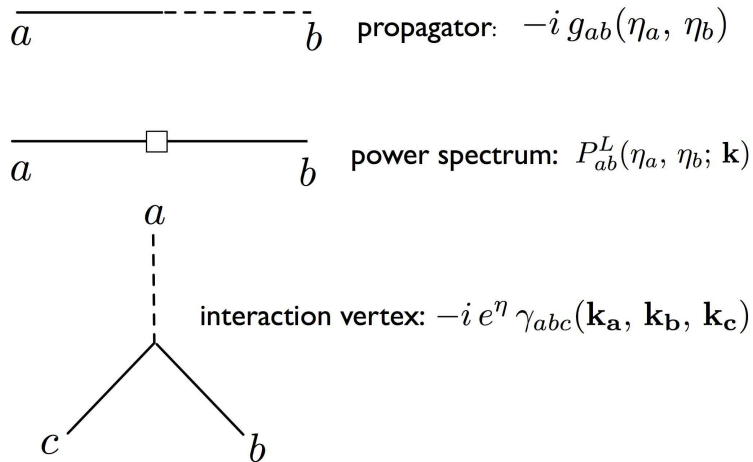


**Figure 1.** The Feynman rules.

legs, respectively. Feynman diagrams constructed by these rules are in one to one correspondence with those considered in [9, 10].

The expression (34) is equivalent, at any order in PT, to

$$Z[J_a, K_b; P^0] = \int \mathcal{D}\varphi_a \mathcal{D}\chi_b \exp \left\{ -\frac{1}{2} \int d\eta_a d\eta_b \chi_a P_{ab}^0 \delta(\eta_a) \delta(\eta_b) \chi_b + i \int d\eta \left[ \chi_a g_{ab}^{-1} \varphi_b - e^\eta \gamma_{abc} \chi_a \varphi_b \varphi_c + J_a \varphi_a + i K_b \chi_b \right] \right\}, \quad (35)$$

which will be useful for the derivation of the RG equations. Notice that the primordial power-spectrum,  $P_{ab}^0$ , is directly coupled to  $\chi$ -fields only, showing the rôle of these fields in encoding the information on the statistics of the initial conditions.

Proceeding on the standard path of field theory, we will also consider the generator of connected Green functions

$$W = -i \log Z, \quad (36)$$

through which we can define expectation values of the fields  $\varphi_a$  and  $\chi_b$  in the presence of sources,

$$\varphi_a[J_c, K_d] = \frac{\delta W[J_c, K_d]}{\delta J_a}, \quad \chi_b[J_c, K_d] = \frac{\delta W[J_c, K_d]}{\delta K_b}. \quad (37)$$

When it is not ambiguous, we will use the same notation for the fields and their expectation values. Full, connected Green functions can be expressed in terms of full propagators and full one-particle irreducible (1PI) Green functions, see for instance Eqs. (44), (45), (46), and (55) below. Therefore it is useful to consider also the generating functional for 1PI Green functions, *i.e.* the effective action. It is defined, as usual, as the Legendre transform of  $W$ ,

$$\Gamma[\varphi_a, \chi_b] = W[J_a, K_b] - \int d\eta d^3\mathbf{k} (J_a \varphi_a + K_b \chi_b). \quad (38)$$

Derivatives of  $\Gamma$  with respect to  $\varphi_a$  and  $\chi_a$  give rise to 1PI  $n$ -point functions. Notice that 1PI functions with all the external legs of type  $\varphi_a$  vanish at any order in PT, *i.e.*

$$\left. \frac{\delta^n \Gamma[\varphi_a, \chi_b]}{\delta \varphi_{a_1}(\eta_1) \cdots \delta \varphi_{a_n}(\eta_n)} \right|_{\varphi_a = \chi_b = 0} = 0 \quad \text{for any } n. \quad (39)$$

Indeed, the contributions to a 1PI  $n$ -point function at  $l$ -loop order contain the product of  $m = n + 2(l - 1)$  basic vertices,

$$\chi \varphi \varphi(\eta_1) \chi \varphi \varphi(\eta_2) \cdots \chi \varphi \varphi(\eta_m). \quad (40)$$

In order to have a 1PI function, at most one of the fields in each vertex can be an ‘external’ field, that is, it is not joined to fields in the other vertices via a propagator ( $\chi - \varphi$  connection) or a power-spectrum ( $\varphi - \varphi$  connection). Moreover, in order to have a  $n$ -point function like Eq. (39), with no  $\chi$ -field as an external field, every  $\chi$  has to be contracted with a  $\varphi$  field belonging to a different vertex, via a retarded propagator. One can then realize that any diagram potentially contributing to (39) contains at least one closed loop of propagators, which vanish due to the presence of the causal  $\theta$ -functions in  $\eta$ .

Considering the second derivatives of the effective action, computed at  $\varphi_a = \chi_a = 0$ , we can then define

$$\begin{aligned} \Gamma_{\varphi_a \varphi_b}^{(2)} &= 0, \\ \Gamma_{\varphi_a \chi_b}^{(2)} &\equiv g_{ba}^{-1} - \Sigma_{\varphi_a \chi_b}, \\ \Gamma_{\chi_a \varphi_b}^{(2)} &\equiv g_{ab}^{-1} - \Sigma_{\chi_a \varphi_b}, \\ \Gamma_{\chi_a \chi_b}^{(2)} &\equiv iP_{ab}^0(k) \delta(\eta) \delta(\eta_b) + i\Phi_{ab}, \end{aligned} \quad (41)$$

where we have isolated the ‘free’ (*i.e.* linear) parts, which can be read off from Eq. (35), and the full, 1PI, two-point functions have been defined as

$$\delta(\mathbf{k}_a + \mathbf{k}_b) \Gamma_{\varphi_a \varphi_b}^{(2)} \equiv \left. \frac{\delta^2 \Gamma[\varphi_a, \chi_b]}{\delta \varphi_a \delta \varphi_b} \right|_{\varphi_a, \chi_b = 0}, \quad (42)$$

and so on.

The full power-spectrum and propagators are given by second derivatives of  $W$ ,

$$\begin{aligned} \left. \frac{\delta^2 W}{\delta J_a \delta J_b} \right|_{J_a, K_b = 0} &\equiv i\delta(\mathbf{k} + \mathbf{k}') P_{ab}, \\ \left. \frac{\delta^2 W}{\delta J_a \delta K_b} \right|_{J_a, K_b = 0} &\equiv -\delta(\mathbf{k} + \mathbf{k}') G_{ab}, \\ \left. \frac{\delta^2 W}{\delta K_a \delta J_b} \right|_{J_a, K_b = 0} &\equiv -\delta(\mathbf{k} + \mathbf{k}') G_{ba}, \\ \left. \frac{\delta^2 W}{\delta K_a \delta K_b} \right|_{J_a, K_b = 0} &= 0. \end{aligned} \quad (43)$$

Using the definitions (37) and (38) one can verify that the four quantities in Eq. (43) form a matrix that is minus the inverse of that formed by the four quantities in (41), which implies that the  $\delta^2 W / \delta K^2$  entry vanishes. We can then express the full propagator

and power-spectrum in terms of the free ones and the ‘self-energies’ appearing in eq (41). Inverting (41) one then gets

$$P_{ab} = P_{ab}^I + P_{ab}^{II}, \quad (44)$$

where

$$\begin{aligned} P_{ab}^I(k; \eta_a, \eta_b) &= G_{ac}(k; \eta_a, 0)G_{bd}(k; \eta_b, 0)P_{cd}^0(k), \\ P_{ab}^{II}(k; \eta_a, \eta_b) &= \int_0^{\eta_a} ds_1 \int_0^{\eta_b} ds_2 G_{ac}(k; \eta_a, s_1)G_{bd}(k; \eta_b, s_2)\Phi_{cd}(k; s_1, s_2) \end{aligned} \quad (45)$$

and

$$G_{ab}(k; \eta_a, \eta_b) = \left[ g_{ba}^{-1} - \Sigma_{\varphi_a \chi_b} \right]^{-1}(k; \eta_a, \eta_b), \quad (46)$$

where the last expression has to be interpreted in a formal sense, that is,

$$G_{ab}(k; \eta_a, \eta_b) = g_{ab}(\eta_a, \eta_b) + \int ds_1 ds_2 g_{ac}(\eta_a, s_1) \Sigma_{\varphi_c \chi_d}(k; s_1, s_2) g_{db}(s_2, \eta_b) + \dots$$

Since our goal is to compute the full non-linear power-spectrum, we see that our task reduces to that of computing the two functions  $G_{ab}$  and  $\Phi_{ab}$ .

#### 4. Renormalization Group Equations

The starting point of our formulation of the RG is a modification of the primordial power-spectrum appearing in the path integral of Eq. (35), as follows,

$$P^0(k) \rightarrow P_\lambda^0(k) = P^0(k) \Theta(\lambda, k), \quad (47)$$

where  $\Theta(\lambda, k)$  is a low-pass filtering function, which equals unity for  $k \ll \lambda$  and zero for  $k \gg \lambda$ . In the computations in this paper we will use a step function,

$$\Theta(\lambda, k) = \theta(\lambda - k), \quad (48)$$

but more smooth behaviors, *e.g.* exponentials or power-laws, can be employed as well.

The modified generating functional, which we now indicate with  $Z_\lambda[J_a, K_b; P^0] \equiv Z[J_a, K_b; P_\lambda^0]$ , describes a fictitious Universe, in which the statistics of the initial conditions is modified by damping all fluctuations with momenta larger than  $\lambda$ . On the other hand, the dynamical content, encoded in the linear propagator and in the structure of the interaction, is left untouched.

In the  $\lambda \rightarrow \infty$  limit all the fluctuations are included, and we recover the physical situation. Increasing the cutoff from  $\lambda = 0$  to  $\lambda \rightarrow \infty$ , the linear and non-linear effect of higher and higher fluctuations is gradually taken into account. This process is described by a RG equation which can be derived by taking the  $\lambda$  derivative of  $Z_\lambda$ ,

$$\begin{aligned} \partial_\lambda Z_\lambda &= -\frac{1}{2} \int \mathcal{D}\varphi_a \mathcal{D}\chi_b \exp \{ \dots \} \times \\ &\quad \int d\eta_a d\eta_b d^3\mathbf{q} \delta(\lambda - q) P_{ab}^0(q) \delta(\eta_a) \delta(\eta_b) \chi_a(\eta_a) \chi_b(\eta_b), \\ &= \frac{1}{2} \int d\eta_a d\eta_b d^3\mathbf{q} \delta(\lambda - q) P_{ab}^0(q) \delta(\eta_a) \delta(\eta_b) \frac{\delta^2 Z_\lambda}{\delta K_b \delta K_a}, \end{aligned} \quad (49)$$

where the meaning of the dots in the argument of the exponential in the first line can be read from Eqs. (35) and (47).

Starting from the equation above and the definition (36) one can obtain the RG equation for  $W_\lambda$ :

$$\partial_\lambda W_\lambda = \frac{1}{2} \int d\eta_a d\eta_b d^3\mathbf{q} \delta(\lambda - q) P_{ab}^0(q) \delta(\eta_a) \delta(\eta_b) \left( i\chi_b \chi_a + \frac{\delta^2 W_\lambda}{\delta K_b \delta K_a} \right). \quad (50)$$

A similar equation can be obtained for the effective action  $\Gamma_\lambda$ . It is convenient to isolate the free from the interacting part, by writing

$$\begin{aligned} \Gamma_\lambda[\varphi, \chi] &= \int d\eta_a d\eta_b d^3\mathbf{q} \left[ \frac{i}{2} \chi_a P_{ab,\lambda}^0(q) \delta(\eta_a) \delta(\eta_b) \chi_b + \chi_a g_{ab}^{-1} \varphi_b \right] \\ &\quad + \Gamma_{\text{int},\lambda}[\varphi, \chi], \\ &\equiv \Gamma_{\text{free},\lambda}[\varphi, \chi] + \Gamma_{\text{int},\lambda}[\varphi, \chi]. \end{aligned} \quad (51)$$

Using (50), one obtains the RG equation for the interacting part of the effective action, which can be written in compact form as

$$\partial_\lambda \Gamma_{\text{int},\lambda} = \frac{i}{2} \text{Tr} \left[ \left( \partial_\lambda \mathbf{\Gamma}_{\text{free},\lambda}^{(2)} \right) \cdot \left( \mathbf{\Gamma}_{\text{free},\lambda}^{(2)} + \mathbf{\Gamma}_{\text{int},\lambda}^{(2)} \right)^{-1} \right], \quad (52)$$

where  $\mathbf{\Gamma}_{\text{free},\lambda}^{(2)}$  is the matrix of second derivatives of the free action (*i.e.* the first terms on the LHS's of Eq. (41), with  $P^0 \rightarrow P_\lambda^0$ ), while  $\mathbf{\Gamma}_{\text{int},\lambda}^{(2)}$  is the matrix of second derivatives of the interacting action, computed at arbitrary field values. The trace indicates  $\eta$  and momentum integrations, as well as summation over the doublet indices of Eq. (9) and over the  $\varphi$  and  $\chi$  field contributions. Notice that, since only the “ $\chi - \chi$ ” entry of  $\mathbf{\Gamma}_{\text{free},\lambda}^{(2)}$  contains the theta function, through the primordial power-spectrum  $P_\lambda^0$  of Eq. (47), this is the only one contributing to the matrix  $\partial_\lambda \mathbf{\Gamma}_{\text{free},\lambda}^{(2)}$ .

In the next section, we will take a closer look at these equations by considering the specific example of the RG equation for the full propagator  $G_{ab,\lambda}$ .

## 5. The propagator and the emergence of an intrinsic UV cutoff

### 5.1. Exact RG equation

The RG equation for the propagator defined in Eq. (43), is derived by taking the appropriate double derivative of. eq (50),

$$\begin{aligned} \partial_\lambda \left. \frac{\delta^2 W_\lambda}{\delta J_a(\mathbf{k}, \eta_a) \delta K_b(\mathbf{k}', \eta_b)} \right|_{J_a, K_b=0} &= -\delta(\mathbf{k} + \mathbf{k}') \partial_\lambda G_{ab,\lambda}(k, \eta_a, \eta_b) = \\ \frac{1}{2} \int d\eta_c d\eta_d d^3\mathbf{q} \delta(\lambda - q) P_{cd}^0(q) \delta(\eta_c) \delta(\eta_d) &\left. \frac{\delta^4 W_\lambda}{\delta J_a \delta K_d \delta K_c \delta K_b} \right|_{J_a, K_b=0}, \end{aligned} \quad (53)$$

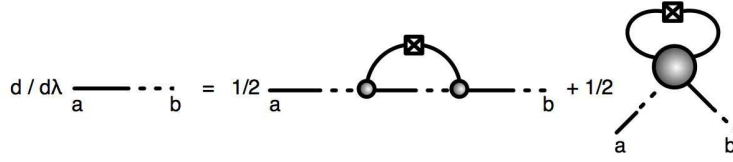


**Figure 2.** RG equation for the propagator  $G_{ab,\lambda}$

were we have used the fact that  $\chi_a$  and  $\delta\chi_a/\delta K_b = \delta^2 W/\delta K_a \delta K_b$  both vanish for vanishing sources  $J_a$  and  $K_b$ . The full connected four-point function,

$$\delta(\mathbf{k}_a + \mathbf{k}_b + \mathbf{k}_c + \mathbf{k}_d) W_{J_a K_b K_c K_d, \lambda}^{(4)} \equiv \frac{\delta^4 W_\lambda}{\delta J_a \delta K_d \delta K_c \delta K_b} \Big|_{J_a, K_b=0}, \quad (54)$$

can be written in terms of full 1PI three and four-point functions and full propagators, as

$$\begin{aligned} & W_{J_a K_b K_c K_d, \lambda}^{(4)}(\mathbf{k}, \eta_a; -\mathbf{k}, \eta_b; \mathbf{q}, \eta_c; -\mathbf{q}, \eta_d) \\ &= \int ds_1 \cdots ds_4 G_{ae, \lambda}(k; \eta_a, s_1) G_{fb, \lambda}(k; s_2, \eta_b) G_{gc, \lambda}(q; s_3, \eta_c) G_{hd, \lambda}(q; s_4, \eta_d) \\ &\times \left\{ \Gamma_{\chi_e \varphi_f \varphi_g \varphi_h, \lambda}^{(4)}(\mathbf{k}, s_1; -\mathbf{k}, s_2; \mathbf{q}, s_3; -\mathbf{q}, s_4) \right. \\ &\quad \left. - \int ds_5 ds_6 G_{li, \lambda}(k - q; s_5, s_6) \right. \\ &\quad \left. 2 \Gamma_{\chi_e \varphi_h \varphi_l, \lambda}^{(3)}(\mathbf{k}, s_1; -\mathbf{q}, s_4; -\mathbf{k} + \mathbf{q}, s_5) \Gamma_{\chi_i \varphi_g \varphi_f, \lambda}^{(3)}(\mathbf{k} - \mathbf{q}, s_6; \mathbf{q}, s_3; -\mathbf{k}, s_2) \right\}, \quad (55) \end{aligned}$$

where we have defined

$$\delta(\mathbf{k}_a + \mathbf{k}_{b_1} + \cdots + \mathbf{k}_{b_{n-1}}) \Gamma_{\chi_a \varphi_{b_1} \cdots \varphi_{b_{n-1}}, \lambda}^{(n)} \equiv \frac{\delta^n \Gamma_\lambda}{\delta \chi_a \delta \varphi_{b_1} \cdots \delta \varphi_{b_{n-1}}} \Big|_{\chi_a, \varphi_b=0}. \quad (56)$$

Inserting the expression above in Eq. (53) we obtain the RG equation represented in Fig. 2, where the thick lines indicate full propagators, dark blobs are full 1PI 3 and 4-point functions, and the crossed box is the *RG kernel*

$$K_{gh, \lambda}(q; s_3, s_4) = G_{gc, \lambda}(q; s_3, 0) G_{hd, \lambda}(q; s_4, 0) P_{cd}^0(q) \delta(\lambda - q). \quad (57)$$

Notice that the kernel can be obtained by deriving w.r.t.  $\lambda$  the  $\theta$  function multiplying the primordial power-spectrum in  $P_\lambda^I$ , see Eqs. (44) and (47).

The RHS of the RG equation is remarkably simple. The two contributions have just the structure of 1-loop diagrams, where the tree-level vertices and propagators have been replaced by full,  $\lambda$ -dependent ones. The same holds true not only in the case of the propagator, but for any other quantity one is interested in.

A recipe can be given to obtain the RG equation for any given quantity:

- write down the *1-loop expression* for the quantity of interest, obtained using *any needed vertex*, (for instance, in Fig. 2, we have not only the vertex  $\chi\varphi\varphi$ , but also  $\chi\varphi\varphi\varphi$ , although it vanishes at tree-level);

- promote the linear propagator, the power-spectrum and the vertices appearing in that expression to full,  $\lambda$ -dependent ones;
- take the  $\lambda$ -derivative of the full expression, by considering only the explicit  $\lambda$ -dependence of the step-function contained in  $P_\lambda^I$ .

It should be emphasized that the RG equations obtained following these rules are *exact*, in the sense that they encode all the dynamical and statistical content of the path-integral (35) or, equivalently, of the continuity, Euler and Poisson equations supplemented by the initial power-spectrum. Despite their 1-loop structure, the complete RG equations resum the theory at any loop order, since the ( $\lambda$ -dependent) full propagators and n-point functions appearing at the RHS contain the contributions of all orders of perturbation theory [12].

### 5.2. Approximations

Different approximation schemes can be attempted. Although the RG equations can be solved perturbatively, thus reproducing the results of PT, they are most indicated for non-perturbative resummations. As a first step, we note that the full 3 and 4-point functions appearing in the RG equation for  $G_{ab,\lambda}$  are also  $\lambda$ -dependent quantities, which can be computed by RG equations, also derived from Eqs. (50, 52). These equations depends, in turn, on full,  $\lambda$ -dependent, functions up to 5 (for the 3-point function) or 6 (for 4-point ones) external legs, which also evolve according to RG equations. Approximations to the full RG flow then amount to truncating the full hierarchy of coupled differential equations, and using some ansatz for the full n-point functions appearing in the surviving equations.

In this paper, we will approximate the full RG flow by keeping the running of the two 2-point functions (propagator and power-spectrum) and keeping the tree-level expression for the trilinear vertex  $\chi\varphi\varphi$ , *i.e.*,

$$\begin{aligned} \Gamma_{\chi_a\varphi_b\varphi_c,\lambda}^{(3)}(\mathbf{k}, s_1; -\mathbf{q}, s_2; -\mathbf{k} + \mathbf{q}, s_3) \\ \simeq -2\delta(s_1 - s)\delta(s_2 - s)\delta(s_3 - s) e^s \gamma_{abc}(\mathbf{k}, -\mathbf{q}, -\mathbf{k} + \mathbf{q}), \end{aligned} \quad (58)$$

while all the other  $n$ -point functions appearing at the RHS of the RG equations are kept to zero, since they vanish at tree-level. In this approximation, only the first diagram on the RHS of Fig. 2 contributes to the running.

### 5.3. 1-loop

Since the RG equations have the structure of 1-loop integrals, PT can be reproduced by solving them iteratively. The  $l$ -th order contribution to a given quantity can be obtained by using up to  $m$ -th order functions (with  $m \leq l - 1$ ) in the RHS of the corresponding RG equation and then closing the loop with the kernel (57), evaluated at order  $l - m - 1$ . So, the computation of the 1-loop contribution to the propagator requires the tree-level

expression for  $W_{J_a K_b K_c K_d, \lambda}^{(4)}$ , obtained by setting all the quantities appearing in Eq. (55) at their tree-level values, that is

$$\begin{aligned} W_{J_a K_b K_c K_d, \lambda}^{(4), \text{tree}} &= -8 \int ds_1 ds_2 e^{s_1 + s_2} g_{hd}(s_1 - \eta_d) g_{gc}(s_2 - \eta_c) g_{ae}(\eta_a - s_1) \\ &\gamma_{ehl}(\mathbf{k}, -\mathbf{q}, -\mathbf{k} + \mathbf{q}) g_{li}(s_1 - s_2) \gamma_{igf}(\mathbf{k} - \mathbf{q}, \mathbf{q}, -\mathbf{k}) g_{fb}(s_2 - \eta_b). \end{aligned} \quad (59)$$

The above expression is  $\lambda$ -independent, so that, once inserted in (53), it allows a straightforward integration in  $\lambda$  from  $\lambda = 0$  to  $\lambda = \infty$ . The initial condition at  $\lambda = 0$  is

$$G_{ab, \lambda=0}(k; \eta_a, \eta_b) = g_{ab}(\eta_a, \eta_b), \quad (60)$$

and the well-known 1-loop result, discussed for instance in Ref. [10], is reproduced $\ddagger$ .

#### 5.4. Large $k$ resummation

A better approximation to the full RG solution is obtained by keeping at least some of the  $\lambda$ -dependence on the RHS of Eq. (53). An analytic result can be obtained in the  $k \gg \lambda$  limit. In this regime, we can still approximate the kernel (57) – which carries momentum  $q = \lambda$  – with its linear expression,

$$K_{gh, \lambda}(q; s_3, s_4) \simeq u_g u_h \theta(s_3) \theta(s_4) P^0(q) \delta(\lambda - q), \quad (61)$$

where we have put the initial conditions on the growing mode, *i.e.*,  $w_a = u_a$ , with  $u_a$  given in Eq. (16).

Starting from Eq. (10) one can verify that, in the  $k \gg q = \lambda$  limit [10],

$$u_f \gamma_{efg}(-\mathbf{k}, \mathbf{q}, \mathbf{k} - \mathbf{q}) \simeq \delta_{eg} \frac{1}{2} \frac{k}{q} \cos \mathbf{k} \cdot \mathbf{q}, \quad (62)$$

so that Eq. (59), once inserted in (53), gives

$$\begin{aligned} \partial_\lambda G_{ab, \lambda}(k; \eta_a, \eta_b) &= -g_{ab}(\eta_a, \eta_b) k^2 \\ &\times \int_{\eta_b}^{\eta_a} ds_2 \int_{\eta_b}^{s_2} ds_1 e^{s_1 + s_2} \int d^3 \mathbf{q} \delta(\lambda - q) P^0(q) \frac{(\cos \mathbf{k} \cdot \mathbf{q})^2}{q^2} \\ &= -g_{ab}(\eta_a, \eta_b) \frac{k^2}{3} \frac{(e^{\eta_a} - e^{\eta_b})^2}{2} \int d^3 \mathbf{q} \delta(\lambda - q) \frac{P^0(q)}{q^2}, \end{aligned} \quad (63)$$

where we have used the following property of the propagators,

$$g_{ae}(\eta_a, s_2) g_{el}(s_2, s_1) = g_{al}(\eta_a, s_1) \theta(\eta_a - s_2) \theta(s_2 - s_1). \quad (64)$$

The equation above is just the large  $k$  limit of the 1-loop result discussed in the previous subsection. Now, a first level of RG improvement consists in promoting the linear propagator  $g_{ab}(\eta_a, \eta_b)$  on the RHS above to the full –  $k$  and  $\lambda$ -dependent – one  $G_{ab, \lambda}(k; \eta_a, \eta_b)$ , while keeping the tree-level expression for the kernel and for the vertices. In this approximation, the RG equation can be integrated analytically, giving

$$G_{ab, \lambda}(k; \eta_a, \eta_b) = g_{ab}(\eta_a, \eta_b) e^{-\frac{k^2}{3} \frac{(e^{\eta_a} - e^{\eta_b})^2}{2}} \int d^3 \mathbf{q} \theta(\lambda - q) \frac{P^0(q)}{q^2}, \quad (65)$$

$\ddagger$  Since our definition of the tree level propagator differs by that of Ref. [10] by a  $e^{-\eta}$  factor, see Eqs. (9, 11), our result for the 1-loop propagator has to be multiplied by  $e^{(\eta_a - \eta_b)}$  before comparing with [10].



**Figure 3.** The infinite class of diagrams resummed by the RG in the approximation leading to Eq. (66).

where the same initial condition at  $\lambda = 0$ , Eq. (60), has been imposed.

In the  $\lambda \rightarrow \infty$  limit, the above expression gives

$$G_{ab,\lambda}(k; \eta_a, \eta_b) = g_{ab}(\eta_a, \eta_b) e^{-k^2 \sigma_v^2 \frac{(e^{\eta_a} - e^{\eta_b})^2}{2}}, \quad (66)$$

where  $\sigma_v^2$  is the velocity dispersion, defined as

$$\sigma_v^2 \equiv \frac{1}{3} \int d^3 \mathbf{q} \frac{P^0(q)}{q^2}. \quad (67)$$

Two comments are in order at this point. First, the RG improvement discussed here has a clear interpretation in terms of PT. Indeed, as shown in [10], the result (66) can be obtained also by resumming the infinite set of diagrams shown in Fig. 3, in which all the power-spectra are directly connected to the propagator line carrying momentum  $k$ . It is amazing how the same result, that in PT requires a careful control of the combinatorics, is here obtained by a simple, 1-loop, integration.

The second, more physical, comment has to do with the dramatic modification of the UV behavior of the resummed propagator w.r.t. the linear one, and on its impact on the RG flow. Indeed, when the propagator of Eq. (66) is employed in the full kernel  $K_{gh,\lambda}$  of Eq.(57), an intrinsic UV cutoff is provided to the RG flow: fluctuations with large momenta are exponentially damped, so that the RG evolution freezes out for  $\lambda \gg e^{-\eta}/\sigma_v$ . This is a genuinely non-perturbative effect, which is masked if one considers PT at any finite order. Indeed, expanding the exponential in Eq. (66), one can see that higher orders in PT are more and more divergent in the UV, obtaining just the opposite behavior. In other words, the full theory is much better behaved in the UV than any of its perturbative approximations.

### 5.5. RG result

An improvement on the approximations leading to Eq. (66) consists in relaxing the  $k \gg \lambda$  condition and in keeping some amount of  $\lambda$ -dependence also in the propagators appearing in the kernel. In this section, we consider the RG equation obtained from Eq. (53) by keeping full,  $\lambda$ -dependent, propagators in Eq. (55), while leaving the vertex functions at their tree-level expression, Eq. (58), with their full-momentum dependence taken into account, that is, not using the approximation in Eq. (62). Consistently, we will also take  $\Gamma_{\chi\varphi\varphi\varphi,\lambda}^{(4)} = 0$ . Higher order approximations, in particular including the running of the vertex, will be considered elsewhere. We have to deal with combinations of full propagators and tree-level vertices as

$$G_{ab,\lambda}(k; s_1, s_2) \gamma_{bfc}(-\mathbf{k}, \mathbf{q}, \mathbf{k} - \mathbf{q}) G_{cd,\lambda}(|\mathbf{k} - \mathbf{q}|; s_2, s_3). \quad (68)$$



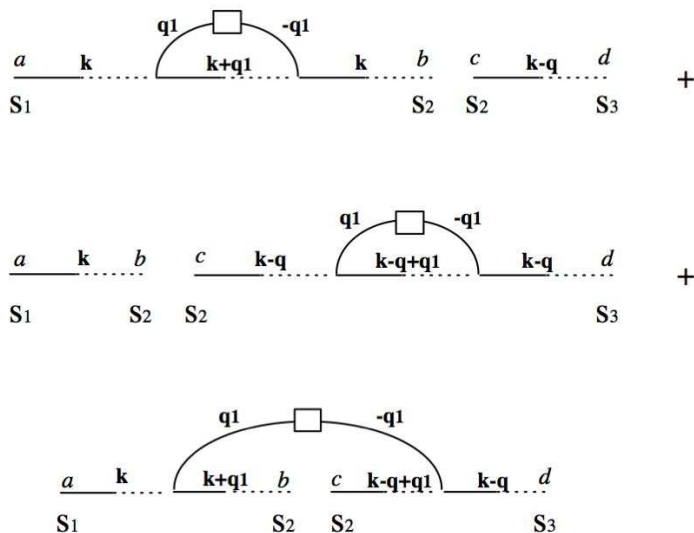


**Figure 4.** The 1-loop contribution to the combination of Eq. (68).

At tree-level, it can be written as

$$\begin{aligned}
 & g_{ab}(s_1, s_2) \gamma_{bfc}(-\mathbf{k}, \mathbf{q}, \mathbf{k} - \mathbf{q}) g_{cd}(s_2, s_3) \equiv \\
 & B_{afc}(\mathbf{k}, \mathbf{q}) g_{cd}(s_1, s_3) \theta(s_1 - s_2) \theta(s_2 - s_3), \quad (69)
 \end{aligned}$$

where the functions  $B_{afc}$  keep track of the full momentum and matrix structure of the tree-level trilinear vertex. The 1-loop contribution to the above combination is given by the sum of the three diagrams in Fig. 4, which in the  $\lambda \ll k$  limit gives

$$\begin{aligned}
 & -\frac{k^2}{3} \frac{(e^{s_1} - e^{s_3})^2}{2} \int d^3 \mathbf{q}_1 \theta(\lambda - q_1) \frac{P^0(q_1)}{q_1^2} \times \\
 & \quad g_{ab}(s_1, s_2) \gamma_{bfc}(-\mathbf{k}, \mathbf{q}, \mathbf{k} - \mathbf{q}) g_{cd}(s_2, s_3) \\
 & = -\frac{k^2}{3} \frac{(e^{s_1} - e^{s_3})^2}{2} \int d^3 \mathbf{q}_1 \theta(\lambda - q_1) \frac{P^0(q_1)}{q_1^2} \times \\
 & \quad B_{afc}(\mathbf{k}, \mathbf{q}) g_{cd}(s_1, s_3) \theta(s_1 - s_2) \theta(s_2 - s_3). \quad (70)
 \end{aligned}$$

Notice that the third diagram in Fig. 4 actually amounts to a 1-loop correction to the trilinear vertex. Repeating the procedure at  $n$ -loops we realize that the corrections can be resummed at any order, giving

$$B_{afc}(\mathbf{k}, \mathbf{q}) g_{cd}(s_1, s_3) e^{-\frac{k^2}{3} \frac{(e^{s_1} - e^{s_3})^2}{2} \int d^3 \mathbf{q} \theta(\lambda - q) \frac{P^0(q)}{q^2}} \theta(s_1 - s_2) \theta(s_2 - s_3), \quad (71)$$

where we recognize the resummed propagator of Eq. (65). Therefore, we learn that the resummation of loop corrections to the combination (69) *is not* the product of two resummed propagators, but a single resummed propagator multiplied by the  $B_{afc}$  matrix. In particular, the dependence on the intermediate ‘time’  $s_2$  appears only in the causal structure enforced by the  $\theta$  functions, while it is absent from the exponential decay factor. We will assume this property to hold also for the RG-resummed propagator, that

is, at the RHS of RG equations we will make use of the relation

$$\begin{aligned} G_{ab,\lambda}(k; s_1, s_2) \gamma_{bfc}(-\mathbf{k}, \mathbf{q}, \mathbf{k} - \mathbf{q}) G_{cd,\lambda}(|\mathbf{k} - \mathbf{q}|; s_2, s_3) = \\ B_{afc}(\mathbf{k}, \mathbf{q}) G_{cd,\lambda}(k; s_1, s_3) \theta(s_1 - s_2) \theta(s_2 - s_3). \end{aligned} \quad (72)$$

Our purpose here will be to go beyond the large  $k$  resummation of Eq. (66). Therefore we will allow an extra  $k$  dependence of the propagator, to be determined by the RG equations. We will therefore use the following ansatz for the full propagator

$$G_{ab,\lambda}(k; s_1, s_2) = H_{ab,\lambda}(k) e^{-k^2 \sigma_v^2 \frac{(e^{s_1} - e^{s_2})^2}{2}}, \quad (73)$$

in which we have factored out the leading time behavior of Eq. (66), and we will use the RG to compute deviations of  $H_{ab,\lambda}(k)$  from unity. Inserting the expression above in the RG equations one obtains, for each external momentum  $k$ , a closed system of four coupled differential equations, one for each component of  $H_{ab,\lambda}$ . In order to simplify it further, we will consider the two combinations  $G_{ab,\lambda} u_b = G_{a1,\lambda} + G_{a2,\lambda}$ , ( $a = 1, 2$ ), therefore we will solve the equations for

$$h_{a,\lambda}(k) = H_{ab,\lambda}(k) u_b, \quad (a = 1, 2). \quad (74)$$

These are given by

$$\partial_\lambda h_{a,\lambda}(k) = -4\pi k^2 S[\lambda; \eta_a, \eta_b] M_a[\lambda/k] P^0(\lambda) \bar{h}_\lambda^2(\lambda) \bar{h}_\lambda(k), \quad (75)$$

where we have approximated all the  $h_{a,\lambda}$ 's appearing at the RHS with

$$h_{a,\lambda}(q) \simeq u_a \bar{h}_\lambda(q) \equiv u_a \frac{h_{1,\lambda}(q) + h_{2,\lambda}(q)}{2}, \quad (76)$$

and we have defined

$$\begin{aligned} M_1[r] = & -\frac{1}{252 r^3} \left[ r(6 - 79r^2 + 50r^4 - 21r^6) + \frac{3}{2}(1 - r^2)^3(2 + 7r^2) \log \left| \frac{1 - r}{1 + r} \right| \right], \\ M_2[r] = & -\frac{1}{84 r^3} \left[ r(6 - 41r^2 + 2r^4 - 3r^6) + \frac{3}{2}(1 - r^2)^3(2 + r^2) \log \left| \frac{1 - r}{1 + r} \right| \right]. \end{aligned} \quad (77)$$

The ‘time’ dependence is contained in the function

$$\begin{aligned} S[\lambda; \eta_a, \eta_b] = & \int_{\eta_b}^{\eta_a} ds_2 \int_{\eta_b}^{s_2} ds_1 e^{s_1 + s_2} e^{-\frac{\lambda^2 \sigma_v^2}{2} [(e^{s_1} - 1)^2 + (e^{s_2} - 1)^2]} \\ = & \frac{\pi}{4\lambda^2 \sigma_v^2} \left\{ \operatorname{erf} \left[ \frac{\lambda \sigma_v (e^{\eta_a} - 1)}{\sqrt{2}} \right] - \operatorname{erf} \left[ \frac{\lambda \sigma_v (e^{\eta_b} - 1)}{\sqrt{2}} \right] \right\}^2, \end{aligned} \quad (78)$$

with erf the ‘error function’,  $\operatorname{erf}(z) = 2\pi^{-1/2} \int_0^z dt e^{-t^2}$ . Notice that in the limit,  $\sigma_v \rightarrow 0$ , we recover the 1-loop behavior,  $S[\lambda; \eta_a, \eta_b] \rightarrow (e^{\eta_a} - e^{\eta_b})^2/2$ .

Notice that, due to the difference between  $M_1[r]$  and  $M_2[r]$ , we have two different equations for  $h_{1,\lambda}$  and  $h_{2,\lambda}$ , *i.e.* two different propagators for the density and the velocity divergence, even if we have approximated them according to Eq. (76) on the RHS.

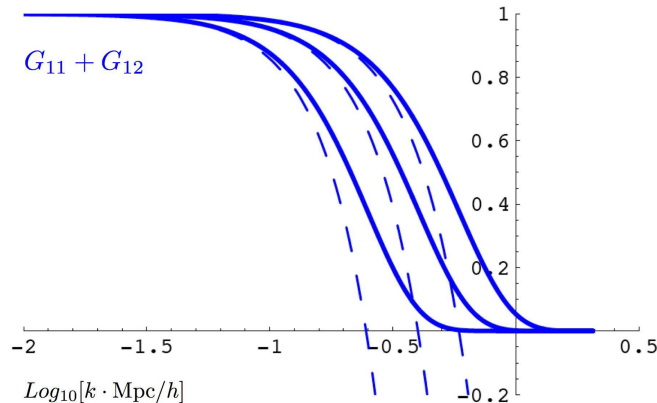


**Figure 5.** The propagator in a  $\Lambda$ CDM model at  $z = 0, 1, 2$ , from left to right. Solid lines represent the results of the integration of Eq. (75). Dashed lines are 1-loop results.

The initial conditions of the RG at  $\lambda = 0$  can be read from Eq. (60), namely

$$h_{a,\lambda=0}(k) = u_a e^{k^2 \sigma_v^2 \frac{(e^{\eta a} - e^{\eta b})^2}{2}}. \quad (79)$$

The RG equations (75), in the limit  $\sigma_v \rightarrow 0$  and  $\bar{h}_\lambda \rightarrow 1$ , give the 1-loop expression for the propagators.

We consider a spatially flat  $\Lambda$ CDM model with  $\Omega_\Lambda^0 = 0.7$ ,  $\Omega_b^0 = 0.046$ ,  $h = 0.72$ ,  $n_s = 1$ . The primordial power-spectrum  $P^0$  is taken from the output of linear theory at  $z_{in} = 80$ , as given by the CAMB Boltzmann code [17].

In Fig. 5 we plot our results for the propagator. Linear theory, Eq. (14), corresponds to  $G_{11} + G_{12} = 1$  for any external momentum  $k$ . The solid lines represent the results of the integration of the RG equation (75) at redshifts  $z = 0, 1, 2$ , from left to right. We plot also the 1-loop results, given by the dashed lines. Notice that, as  $k$  grows, the latter become negative, signaling the breakdown of the perturbative expansion.

As one can see, the damping of the propagator for large  $k$ , that we obtained in the large momentum approximation leading to Eq. (66), is exhibited also by the solutions of the more accurate RG equations (75).

## 6. The power-spectrum

The full power-spectrum has the structure of Eqs. (44, 45), where the primordial power-spectrum  $P^0$  contained in  $P_{ab}^I$  has been multiplied by  $\theta(\lambda - k)$ , as in Eq. (47), and the full propagators and the function  $\Phi_{ab}$  are now  $\lambda$ -dependent quantities. The RG evolution of the first term,  $P_{ab,\lambda}^I$ , is completely determined by that of the full propagator, that we have computed in the previous section. Our task now reduces to computing the

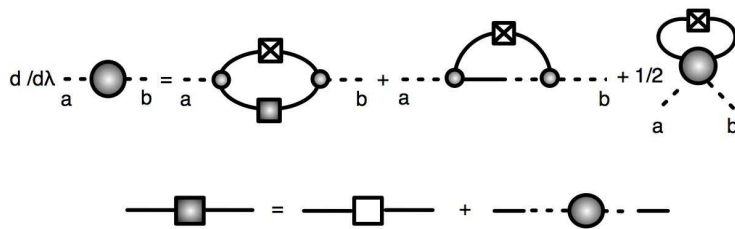


**Figure 6.** RG equation for  $\Phi_{ab,\lambda}$

evolution of  $P_{ab,\lambda}^{II}$ ,

$$\begin{aligned} \partial_\lambda P_{ab,\lambda}^{II}(k; \eta_a, \eta_b) = & \\ & \int_0^{\eta_a} ds_1 \int_0^{\eta_b} ds_2 \left[ \partial_\lambda G_{ac,\lambda}(k; \eta_a, s_1) G_{bd,\lambda}(k; \eta_b, s_2) \Phi_{cd,\lambda}(k; s_1, s_2) \right. \\ & + G_{ac,\lambda}(k; \eta_a, s_1) \partial_\lambda G_{bd,\lambda}(k; \eta_b, s_2) \Phi_{cd,\lambda}(k; s_1, s_2) \\ & \left. + G_{ac,\lambda}(k; \eta_a, s_1) G_{bd,\lambda}(k; \eta_b, s_2) \partial_\lambda \Phi_{cd,\lambda}(k; s_1, s_2) \right]. \quad (80) \end{aligned}$$

The missing element is the running the 1PI two-point function,  $\Phi_{ab,\lambda}$ , which can be obtained by the recipe given in sect. 5 and is represented graphically in Fig. 6. The dark box represents the full,  $\lambda$ -dependent, power-spectrum. Notice that, besides the  $\chi\varphi\varphi$  vertex, also  $\chi\chi\varphi$  and  $\chi\chi\varphi\varphi$  appear in the full RG equation.

We will stick to the same truncation scheme considered in the computation of the propagator, that is, we will allow running propagator and power-spectrum and will keep the vertices at tree-level. In this approximation, only the first diagram at the RHS of Fig. 6 contributes to the running, and the RG equation is

$$\begin{aligned} \partial_\lambda \Phi_{ab,\lambda}(k; s_1, s_2) = & 4 e^{s_1+s_2} \int d^3\mathbf{q} \delta(\lambda - q) P_{dc,\lambda}^I(q; s_1, s_2) \times \\ & P_{fe,\lambda}^I(|\mathbf{q} - \mathbf{k}|; s_1, s_2) \gamma_{adf}(\mathbf{k}, -\mathbf{q}, -\mathbf{k} + \mathbf{q}) \gamma_{bce}(-\mathbf{k}, \mathbf{q}, \mathbf{k} - \mathbf{q}). \quad (81) \end{aligned}$$

We will proceed along the same lines we followed in the computation of the propagator. Namely, we will again make use of the ansatz (73) for the propagator, and of the approximation (76) for those propagators appearing on the RHS of the RG equations. As a consequence, the contribution  $P_{ab,\lambda}^I$  to the power-spectrum will be approximated, at the RHS, as

$$P_{ab,\lambda}^I(q; \eta_a, \eta_b) \simeq u_a u_b \bar{h}_\lambda^2(q) P^0(q) e^{-q^2 \sigma_v^2 \frac{(e^{\eta_a} - 1)^2 + (e^{\eta_b} - 1)^2}{2}}. \quad (82)$$

To reduce the number of equations, we focus on the evolution of an ‘average’  $P_{ab,\lambda}^{II}$ , defined as

$$\bar{P}_\lambda^{II} \equiv \frac{1}{4} u_a u_b P_{ab,\lambda}^{II}. \quad (83)$$

Since  $P_{ab,\lambda}^{II}$  evaluated at  $s_1$  and  $s_2$  appears on the RHS of Eq. (81) we need it at generic time arguments. While, in principle, the complete time dependence could be obtained from Eq. (80) itself, it would be in practice extremely time-consuming. Therefore, we will make two different *ansatze* on the time dependence of the  $P_{ab,\lambda}^{II}$  appearing on the

RHS of (81), verifying *a posteriori* the stability of our results with respect to the two different choices. The first ansatz is inspired by the analogy with Eq. (82),

$$\bar{P}_\lambda^{II}(q; \eta_a, \eta_b) = \bar{P}_\lambda^{II}(q; s_1, s_2) e^{-q^2 \sigma_v^2 \frac{(e^{\eta_a} - e^{s_1})^2 + (e^{\eta_b} - e^{s_2})^2}{2}}, \quad (84)$$

while the second one is simply

$$\bar{P}_\lambda^{II}(q; \eta_a, \eta_b) = \bar{P}_\lambda^{II}(q; s_1, s_2). \quad (85)$$

The comparison between the power-spectra obtained with these two choices will be given in Fig. 10 below.

Moreover, we will compute the power-spectrum at equal times, that is  $\eta_a = \eta_b = \eta$ .

Inserting the expressions above in (81), and then contracting Eq. (80) with  $u_a u_b$ , we arrive, after performing the integrations in  $s_1, s_2$ , and  $\mathbf{q}$ , to

$$\begin{aligned} \partial_\lambda \bar{P}_\lambda^{II}(k; \eta) &= -4\pi k^2 \bar{h}_\lambda^2(\lambda) P^0(\lambda) \left\{ S[\lambda; \eta, 0] u_a M_a[\lambda/k] \bar{P}_\lambda^{II}(k; \eta) \right. \\ &\quad - \frac{1}{2k} \int_{|k-\lambda|}^{k+\lambda} dp \left[ \theta(\lambda - p) \bar{h}_\lambda^2(p) U(\lambda^2, k^2, p^2; \eta) P^0(p) \right. \\ &\quad \left. \left. + U(k^2, \lambda^2, -p^2; \eta) \bar{P}_\lambda^{II}(p; \eta) \right] \frac{(2k^4 - 3(p^2 - \lambda^2)^2 + k^2(p^2 + \lambda^2))^2}{100k^2 p^3 \lambda^3} \right\}, \quad (86) \end{aligned}$$

with the initial condition

$$\bar{P}_{\lambda=0}^{II}(k; \eta) = 0. \quad (87)$$

The function  $U$  is defined as

$$\begin{aligned} U(\lambda^2, k^2, p^2; \eta) &= \left[ \int_0^\eta ds e^s e^{-\frac{(\lambda^2 + p^2)\sigma_v^2}{2}(e^s - 1)^2 - \frac{k^2\sigma_v^2}{2}(e^\eta - e^s)^2} \right]^2 \\ &= \frac{\pi}{2\sigma_v^2} \frac{1}{\lambda^2 + k^2 + p^2} e^{-\frac{k^2(\lambda^2 + p^2)\sigma_v^2}{\lambda^2 + k^2 + p^2}(e^\eta - 1)^2} \times \\ &\quad \left\{ \operatorname{erf} \left[ \frac{k^2\sigma_v}{\sqrt{\lambda^2 + k^2 + p^2}} \frac{(e^\eta - 1)}{\sqrt{2}} \right] + \operatorname{erf} \left[ \frac{(\lambda^2 + p^2)\sigma_v}{\sqrt{\lambda^2 + k^2 + p^2}} \frac{(e^\eta - 1)}{\sqrt{2}} \right] \right\}^2, \quad (88) \end{aligned}$$

and, in the  $\sigma_v \rightarrow 0$  limit it goes to  $(e^\eta - 1)^2$ . In this limit, and setting  $\bar{P}_\lambda^{II} = 0$  in the RHS, the integration of Eq. (86) gives the 1-loop result.

In Fig. 7 we plot our results for the power-spectrum (solid lines), in the momentum range relevant for the BAO, at  $z = 0, 1$ , and  $2$ , from bottom to top. Long-dashed lines and dot-dashed ones correspond to the two contributions  $P_{11}^I$  and  $P_{11}^{II}$  to the full power-spectrum [see Eqs. (44, 45)], respectively. The results of linear theory are given by the short-dashed lines. Notice the decrease of the contribution  $P_{11}^I$  for growing  $k$ , due to the damping of the propagators seen in Fig. 5. For the lower peaks, this is partially compensated by the contribution  $P_{11}^{II}$ , so that the full power-spectrum approximately tracks the linear theory result up to  $k \lesssim 0.12 h/\text{Mpc}$  (for  $z = 0$ ). At first sight, this agreement could lead to the conclusion that non-linearities are small in this range of wavenumbers. However, this is the effect of a fortuitous cancellation between two non-linear effects, *i.e.* the damping of  $P_{11}^I$  and the contribution  $P_{11}^{II}$ , which – taken separately – are of order 40% of the linear contribution.

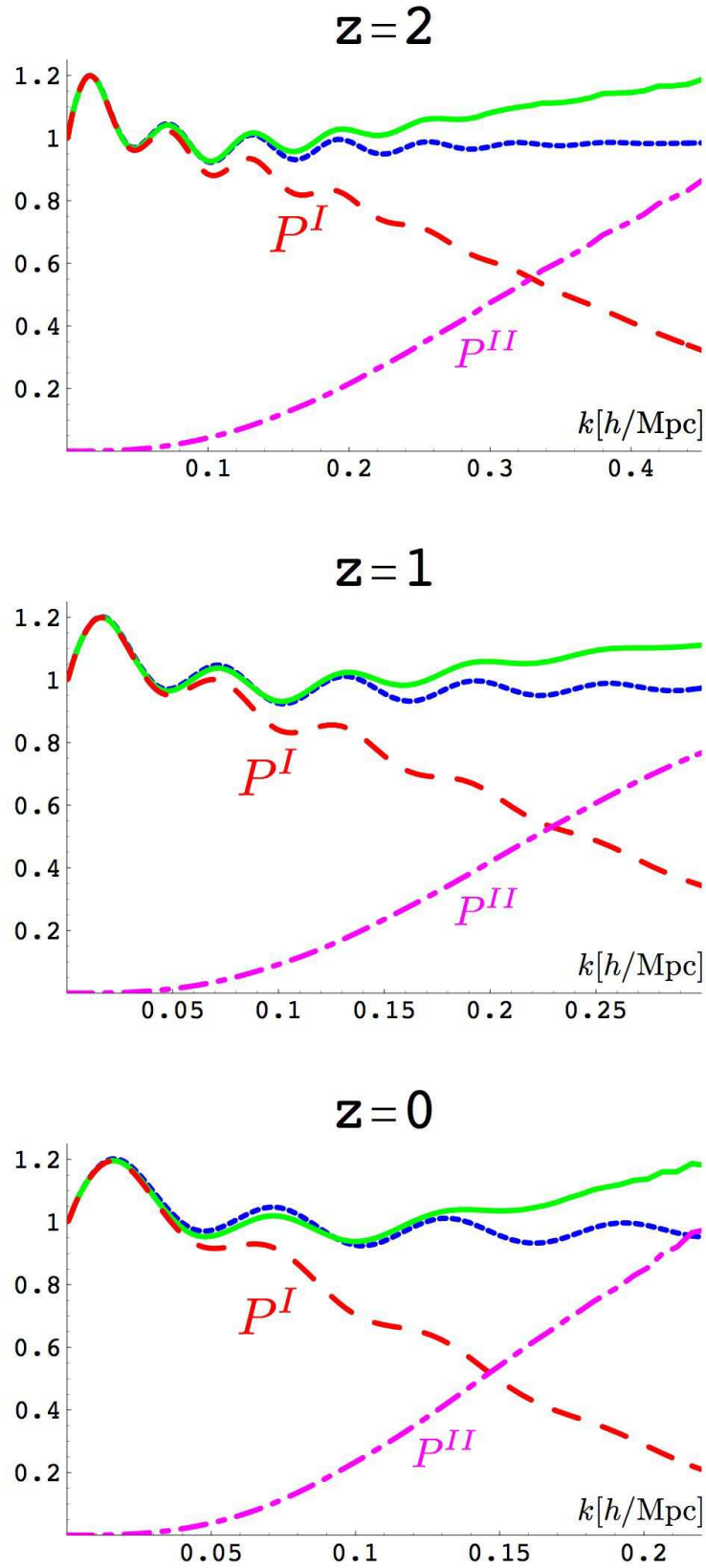


**Figure 7.** The contributions of  $P_{11}^I$  (long-dashed line) and  $P_{11}^{II}$  (dot-dashed) to the total power-spectrum,  $P_{11} = P_{11}^I + P_{11}^{II}$  (solid). The linear theory result (short-dashed) is also shown.

In Figs. 8, 9 we compare our results (solid lines) with two sets of N-body simulations appeared in the literature, that is with those of refs.[4] and [5], respectively. Since the two sets of simulations correspond to two slightly different cosmologies (see the figure captions), it is not possible to draw them on the same plot. The short-dashed lines correspond to linear theory and the long-dashed ones to 1-loop PT (which, at  $z = 0$  in Fig. 8 has been truncated for  $k \gtrsim 0.17 \text{ h/Mpc}$ , where  $P_{11}^I$  takes negative values, signaling the breakdown of the perturbative expansion). The black squares are taken from the N-body simulations. In Fig.9 we also plot the results from the halo-model approach of Ref. [8]. To enhance the BAO feature, each power-spectrum has been divided by the linear one, in a model without baryons [18]. In the peak region, our RG results agree with those of N-body simulations to a few percent accuracy down to redshift  $z = 0$ , where linear and 1-loop PT badly fail. Thus, the dynamical behavior in this momentum range appears to be captured fairly well by the approximations implemented by our approach, namely the ‘single stream approximation’, leading to Eq. (11), and the non-linear corrections of the two-point functions only, i.e. the propagator and the power-spectrum.

An estimate of the accuracy and range of validity of the different approximations described so far can be made by improving the level of truncations, the first step being taking into account the running of the trilinear vertex. Alternatively, one can change the *ansatze* for the compositions between full propagators, Eq. (72) or for the time dependence of the  $P^{II}$  contribution to the power-spectrum, Eqs.(84, 85). In Fig. 10 we compare the results for the power-spectrum obtained by using the two different approximations for  $P^{II}$ . As one can see, the results are quite stable in the range of momenta relevant for the BAO, that is, for  $k \lesssim 0.25 \text{ h Mpc}^{-1}$ . For higher momenta, the power-spectrum obtained from the RG is suppressed with respect to the one from the N-body simulations. The main origin of this effect is the progressive failure of the composition law of Eq. (72) for large values of the combination  $\sigma_v^2 k^2 (e^{s_1} - e^{s_3})^2$ . In order to improve this approximation, one could split into small steps the time integrations, that now are made in one single step from  $\eta_i = \log D^+(0)/D^+(z_{in})$  down to  $\eta = \log D^+(z)/D^+(z_{in})$ , with  $z_{in}$  typically larger than 30. At each step the renormalized power-spectrum would be assumed as the new ‘primordial’ one. In this way, we expect to reduce considerably the dependence on the different approximations to the exact time-dependence of the propagator and of  $P^{II}$ . The implementation of this procedure, together with the inclusion of the running of the vertex, will be the subject of future work.

## 7. Conclusions

In this paper we have explored the possibility of using RG techniques as a computational tool to solve the continuity and Euler equations (5) non-perturbatively. The need of a non-perturbative approach as one moves towards high wavenumbers is manifest if one considers the propagator. In this case, the  $n$ -th order perturbative contribution diverges

as  $k^{2n}$ , while the full result goes exponentially to zero, as shown in Ref. [10] and in this paper. As a consequence, the full RG flow freezes at large momenta, and the results are insensitive to the details of the matter distribution at small scales, an effect which cannot be seen at any order in PT.

Non-linear effects contribute sizeably to the power-spectrum in the BAO momentum range (see Fig. 7), and their reliable estimation is completely out of reach of PT, for  $z \lesssim 1$  (Fig.8). We have approximated the RG equations by renormalizing only the 2-point functions, *i.e.* the power-spectrum and the propagator, while keeping the trilinear interaction frozen at its tree-level value. This approximation performs surprisingly well, and our results agree with those of the N-body simulation of [4].

In view of other applications requiring the power-spectrum at higher wavenumbers, like *e.g.* weak gravitational lensing, the RG performance can be systematically improved by increasing the level of truncation of the full tower of differential equations. The next step will be the inclusion of the running of the trilinear vertex, which will also allow a computation of non-linear effects on the bispectrum.

Further applications of our RG approach include the computation of higher-order statistics, the analysis of the possible effects of initial non-Gaussianity on non-linear scales and the effect of a non-vanishing stress-tensor  $\sigma_{ij}$ .

The extension of the present approach to cosmological models including dynamical dark energy will also be the subject of future work.

## Acknowledgments

We thank E. Komatsu and M. White, for providing us with the N-body data of Refs. [5] and [4] respectively, N. Bartolo, P. McDonald and M. Viel, for discussions. M.P. thanks the Galileo Galilei Institute for Theoretical Physics for hospitality during the initial stages of this work.

## References

- [1] D. J. Eisenstein, W. Hu and M. Tegmark, *Astrophys. J.* **504**, L57 (1998); H. J. Seo and D. J. Eisenstein, arXiv:astro-ph/0701079.
- [2] D. J. Eisenstein *et al.* [SDSS Collaboration], *Astrophys. J.* **633**, 560 (2005); G. Huetsi, *Astron. Astrophys.* **449**, 891 (2006); N. Padmanabhan *et al.* [SDSS Collaboration], astro-ph/0605302; C. Blake, A. Collister, S. Bridle and O. Lahav, astro-ph/0605303.
- [3] A. Cooray, W. Hu, D. Huterer and M. Joffe, *Astrophys. J.* **557**, L7 (2001); W. Hu and Z. Haiman, *Phys. Rev. D* **68**, 063004 (2003); C. Blake and K. Glazebrook, *Astrophys. J.* **594**, 665 (2003); H. J. Seo and D. J. Eisenstein, *Astrophys. J.* **598**, 720 (2003) K. Glazebrook and C. Blake, *Astrophys. J.* **631**, 1 (2005) R. Angulo, C. M. Baugh, C. S. Frenk and C. G. Lacey, arXiv:astro-ph/0702543.
- [4] E. Huff, A. E. Schulz, M. White, D. J. Schlegel and M. S. Warren, *Astropart. Phys.* **26**, 351 (2007).
- [5] D. Jeong and E. Komatsu, *Astrophys. J.* **651**, 619 (2006).
- [6] F. Bernardeau, S. Colombi, E. Gaztanaga and R. Scoccimarro, *Phys. Rept.* **367**, 1 (2002).
- [7] J. A. Peacock and S. J. Dodds, *Mon. Not. Roy. Astron. Soc.* **280**, L19 (1996).
- [8] R. E. Smith, *et al.*, *Mon. Not. Roy. Astron. Soc.* **341** 1311 (2003).



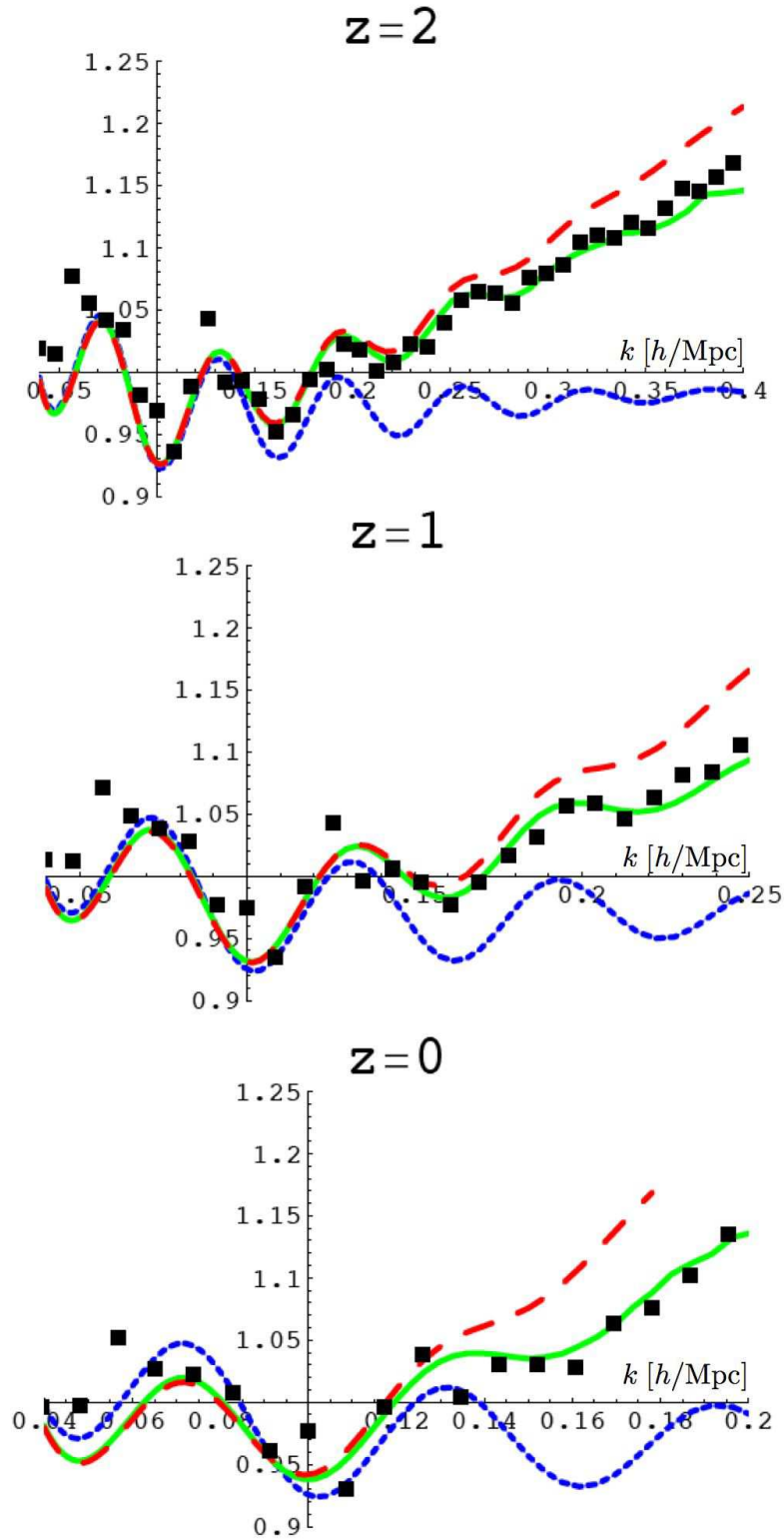


**Figure 8.** The power-spectrum at  $z = 2, 1, 0$ , as given by the RG (solid line), linear theory (short-dashed), 1-loop PT (long-dashed), and the N-body simulations of [4] (squares). The background cosmology is a spatially flat  $\Lambda$ CDM model with  $\Omega_{\Lambda}^0 = 0.7$ ,  $\Omega_b^0 = 0.046$ ,  $h = 0.72$ ,  $n_s = 1$ .

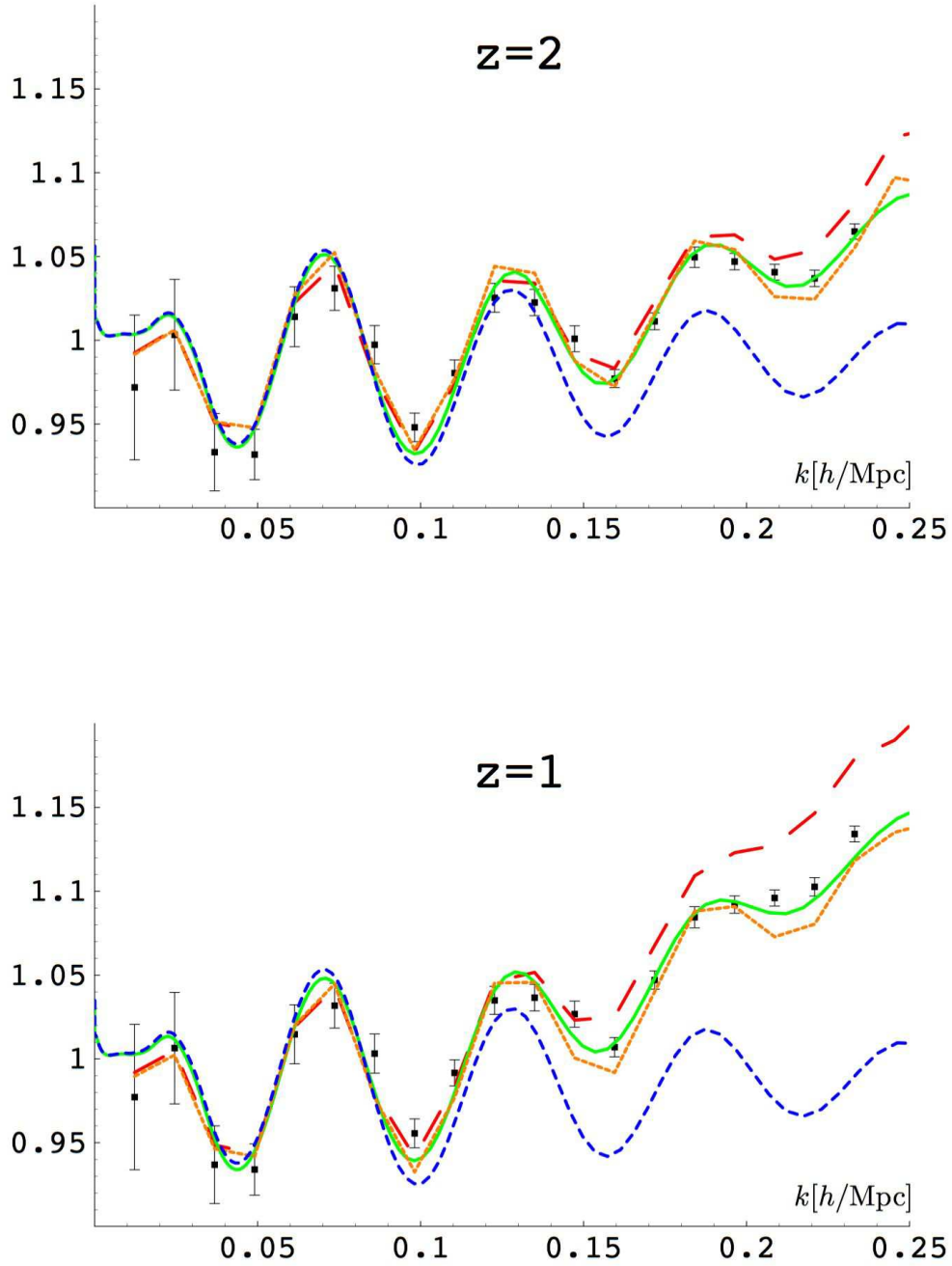


**Figure 9.** The power-spectrum at  $z = 2, 1$ , as given by the RG (solid line), linear theory (short-dashed), 1-loop PT (long-dashed), the halo approach of Ref. [8] (very short-dashed), and the N-body simulations of [5] (squares). The background cosmology is a spatially flat  $\Lambda$ CDM model with  $\Omega_{\Lambda}^0 = 0.73$ ,  $\Omega_b^0 = 0.043$ ,  $h = 0.7$ ,  $n_s = 1$

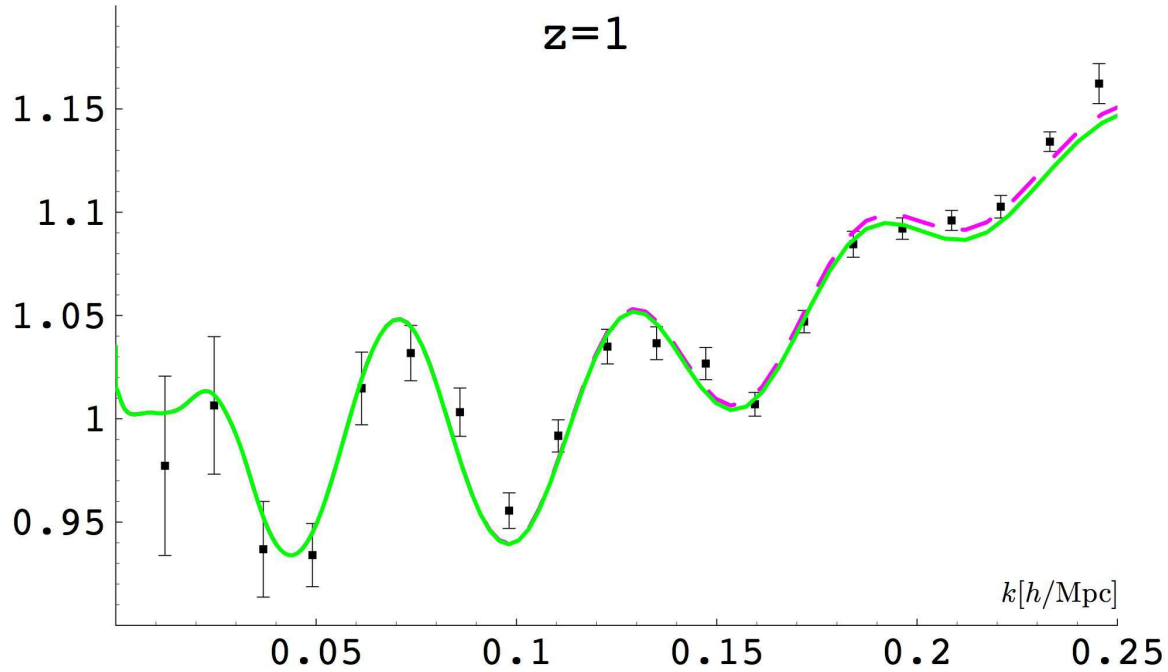


**Figure 10.** The power-spectrum at  $z = 1$ , as given by the RG with two different *ansatze* for the time-dependence of  $P_{\lambda}^{II}$ . The dashed and solid lines were obtained using Eqs. (84) and (85), respectively. Dots with error bars are taken from the simulations of Ref. [5].

- [9] M. Crocce and R. Scoccimarro, Phys. Rev. D **73**, 063519 (2006).
- [10] M. Crocce and R. Scoccimarro, Phys. Rev. D **73**, 063520 (2006).
- [11] P. J. E. Peebles, Astrophys. J. **297**, 350 (1985); J. Gaite, Int. J. Mod. Phys. A **16**, 2041 (2001); J. Gaite and A. Dominguez, arXiv:astro-ph/0610886; P. McDonald, Phys. Rev. D **75**, 043514 (2007); P. Valageas, Astron. Astrophys. **421**, 23 (2004); P. Valageas, arXiv:astro-ph/0611849; T. Padmanabhan and S. Ray, Mon. Not. Roy. Astron. Soc. Lett. **372**, L53 (2006); N. Afshordi, Phys. Rev. D **75**, 021302 (2007).
- [12] For applications of the Wilsonian RG in quantum field theory and statistical physics, see J. Polchinski, Nucl. Phys. B **231**, 269 (1984); M. Bonini, M. D’Attanasio and G. Marchesini, Nucl. Phys. B **409**, 441 (1993); T. R. Morris, Int. J. Mod. Phys. A **9**, 2411 (1994); M. D’Attanasio and M. Pietroni, Nucl. Phys. B **472**, 711 (1996); J. Berges, N. Tetradis and C. Wetterich, Phys. Rept. **363**, 223 (2002).
- [13] S. Matarrese and M. Pietroni, astro-ph/0702653.
- [14] A. Nusser and J.M. Colberg, Mon. Not. Roy. Astron. Soc. **294**, 457 (1998).
- [15] E. Calzetta and B. L. Hu, Phys. Rev. D **37**, 2878 (1988).
- [16] For the use of path integral methods in classical theories, see E. Gozzi, M. Reuter and W. D. Thacker, Phys. Rev. D **40**, 3363 (1989); R. Penco and D. Mauro, Eur. J. Phys. **27**,

1241 (2006).

[17] A. Lewis, A. Challinor and A. Lasenby, *Astrophys. J.* **538**, 473 (2000).

[18] D. J. Eisenstein and W. Hu, *Astrophys. J.* **496**, 605 (1998).